Accurate band structures and effective masses for InP, InAs, and InSb using hybrid functionals

Yoon-Suk Kim,* Kerstin Hummer, and Georg Kresse
Department of Computational Materials Physics, Universität Wien, Sensengasse 8/12, A-1090 Wien, Austria
(Received 28 April 2009; published 13 July 2009)

The band structures of In X (X=P, As, and Sb) are calculated using the hybrid HSE06 functional and GW with spin-orbit coupling effects included up to second order. Conventional local or semilocal density functionals predict an incorrect band ordering for InAs and InSb when spin-orbit coupling is included. We show that inclusion of one quarter of the exact exchange allows us to predict very accurate band gaps for InP, InAs, and InSb, i.e., 1.48, 0.42, and 0.28 eV, respectively, in good agreement with recent experiments. Furthermore, calculated effective masses for the conduction band (electron) and the valence band (heavy-hole, light-hole, and split-off band) are in fairly good agreement, whereas the values obtained using semilocal functionals deviate significantly from experiment even for InP. The calculated Luttinger parameters are also in reasonable agreement with experiment, although a tendency toward underestimation is observed with increasing anion mass. This underestimation is shown to be partially related to a tendency to overestimate the band gaps for the heavier elements using the particular hybrid functional used in this study. By adjusting the screening parameter in the hybrid functional, agreement with the experimental band gap can be achieved, but even then the Luttinger parameters are 15% smaller than the experimental values for InAs and InSb.

DOI: 10.1103/PhysRevB.80.035203 PACS number(s): 71.15.Mb, 71.55.Eq, 71.70.Ej

I. INTRODUCTION

The III-V zinc-blende semiconductors, In X (X=P, As, and Sb), have recently received much attention since they have potential to be employed as base materials for light-emitting diodes, infrared detectors, and spintronic devices, e.g., quantum-dot and quantum-well applications.[1–3] The materials have been the subject of a large variety of experimental as well as theoretical investigations.[4–6] Generally, density functional theory (DFT) is found to describe reasonably well the structural properties, such as lattice constants and bulk moduli. However, for the description of the electronic properties of In X semiconductors, e.g., band gaps, spin-orbit splittings, and effective masses, etc., Kohn-Sham DFT yields unsatisfactory results. For InAs and InSb, the band ordering at the Γ point is incorrect, and resultantly effective masses are crossly wrong.[7,8] Two approaches hold the promise to cure these problems. Hybrid functionals that admix a fixed fraction of the nonlocal exchange are one simple but fairly efficient solution;[9] the more systematic and rigorous approach, however, are the quasiparticle Green's-function-based methods, such as the GW approximation.[10]

Describing the band structure of the narrow band-gap semiconductor, In X, poses many challenges. Since the crystal structure of In X semiconductors, zinc blende, lacks inversion symmetry, Dresselhaus spin splitting is observed at the valence band maximum and the conduction band minimum.[11] Spin-orbit coupling (SOC) and the lack of inversion symmetry splits the originally threefold-degenerated occupied anion p states into one split-off state, a light-hole, and one heavy-hole band.[12] A further complication is that the electronic properties are strongly influenced by the interaction between the In d semicore electrons, which form shallow bands close to the valence band region. For an accurate evaluation of the band structure the localized semicore In d states need to be treated as valence states and SOC needs to be taken into account.

The most thorough theoretical study of In X has been performed by Cardona *et al.* using the linearized muffin-tin-orbital (LMTO) method.[12] In that study, the muffin-tin potentials were semiempirically adjusted by adding a sharply peaked potential at the atomic sites in order to fit the experimental band gaps. In this sense that study was not parameter free. On the other hand, very recent state of the art self-consistent GW calculations also failed to predict accurate band gaps and effective masses without adjusting the self-energy operator.[13] Our aim is to determine how well hybrid functionals perform in describing subtle details of the band structure. To this end, the projector-augmented-wave (PAW) method is used to investigate the structural and electronic properties of In X narrow band-gap semiconductors. Spin-orbit coupling effects are included self-consistently up to second order inside the PAW spheres, and hybrid as well as semilocal functionals are used. The band gaps are also calculated in the GW approximation, starting from hybrid functionals.

II. COMPUTATIONAL DETAILS

The results of this study were obtained using the Vienna *ab initio* simulation package (VASP).[14] The PAW method[15] as implemented in the VASP code[16] was utilized to describe the interaction between the ionic cores and the valence orbitals. The generalized gradient approximation as parametrized by Perdew, Burke, and Ernzerhof (PBE) (Ref. 17) was employed to describe the exchange-correlation energy in the standard DFT calculations. In order to get a better description of the band gaps, hybrid functionals[18] as well as the GW (Refs. 19 and 20) method were used. The use of hybrid functionals is motivated by the observation that the hybrid functional proposed by Heyd, Scuseria, and Ernzerhof (HSE) (Ref. 9) is performing extremely well for the band gap of semiconductors.[21–24] Remarkably, with the exception of the lead chalcogenides, effective masses have not yet been pre-

dicted using hybrid functionals.[24] An evaluation of the effective masses for challenging materials, such as the In X semiconductors, might contribute to the acceptance of hybrid functionals for the modeling of semiconductors.

In standard DFT calculations, both the exchange (E_x) and the correlation (E_c) energies are treated by a local or semilocal approximation. Due to self-interaction errors and the lack of an integer discontinuity of the exchange-correlation energy upon changing the number of electrons, standard Kohn-Sham DFT band gaps are always too small.[25,26] On the other hand, the Hartree-Fock (HF) method predicts much too large band gaps, which is attributed to the lack of correlation, and to the fact that the unoccupied orbitals experience the repulsive Hartree potential only. It has been demonstrated by Muscat *et al.* that hybrid functionals including one quarter of the exact exchange can yield very reasonable band gaps for semiconductors,[27] an observation that has since then been confirmed by many other studies,[9,22] including some very challenging small gap solids such as lead chalcogenides[24] or ternary and quaternary compounds.[28]

The HSE functional, used in the present work, employs a screened short-range HF exchange instead of the full exact HF exchange. This has two main advantages. First, HSE reduces the computational demands: since the long-range tail of the Coulomb kernel is removed, a more rapid convergence of the exchange interaction with the number of k points is obtained than for the bare HF exchange.[22,29] Second, the screening is more effective at longer wavelength and resultantly in materials with a larger lattice constant and a larger characteristic wavelength at the Fermi level less nonlocal exchange is included close to the Fermi level. This "automatism" allows an accurate prediction of the band gaps within one series (for Si-Sn, see Ref. 30).

For the HSE functional, the exchange-correlation energy is defined as

$$E_{xc}^{HSE} = E_x^{DFT}(\mu) - \tfrac{1}{4}E_x^{DFT,SR}(\mu) + \tfrac{1}{4}E_x^{HF,SR}(\mu) + E_c^{DFT}, \quad (1)$$

where the screening parameter μ defines the range separation and is empirically set to 0.2–0.3 Å^{-1}. $E_x^{DFT,SR}$ is a density functional for the short-range part of the exchange energy, whereas $E_x^{HF,SR}(\mu)$ is the exact nonlocal exchange evaluated with a short-range screened Coulomb kernel. In this work, μ was consistently set to $\mu=0.2$ Å^{-1} (HSE06 scheme) for both the HF and the DFT parts.[31] The interaction range of the SR nonlocal exchange ($\pi/\mu \approx 15$ Å) is over several nearest neighbors and thus considerably more long ranged than in conventional semilocal functionals. More details about the implementation of hybrid functionals in the VASP program can be found in Refs. 18 and 22.

The present calculations use scalar-relativistic PAW potentials, where both the core as well as the valence orbitals are treated using a scalar relativistic Hamiltonian. The spin-orbit term was evaluated using the well-known second-order approximation[32]

$$H^{SOC} = \frac{\hbar}{4m^2c^2}\sum_d (\nabla V^{KS} \times p)\cdot\sigma, \quad (2)$$

where V^{KS} is the Kohn-Sham potential and p the momentum operator. The corresponding terms are only large inside the PAW spheres and can be rewritten as

TABLE I. Potential parameters of the projector-augmented-wave method (see text for details).

Elements	Valence states	Local potential	R_{core} (a.u.)	E_{cut} (eV)
In	$4d^{10}5s^25p^1$	$4f$	2.5	240
P	$3s^23p^3$	$3d$	1.9	270
As	$4s^24p^3$	$4f$	2.1	209
Sb	$5s^25p^3$	$5f$	2.3	173

$$H^{SOC} = \frac{\hbar^2}{4m^2c^2}\frac{1}{r}\frac{\partial V_0^{KS}}{\partial r}\vec{L}\cdot\vec{s}, \quad (3)$$

where $\vec{L}$ is the angular-momentum operator, $\vec{s}$ are the Pauli spin matrices, and V_0^{KS} is the spherical part of the all-electron Kohn-Sham potential inside the PAW spheres. The one-center Hamiltonian for the all-electron wave functions is then given by

$$H^{DFT+SOC} = \frac{p^2}{2m} + V^{KS} + H^{SOC}. \quad (4)$$

The matrix elements of the Hamiltonian are evaluated using atomic all-electron orbitals determined for the atoms using a scalar-relativistic Hamiltonian. In the following, it is noted that this second-order form for the SOC yields diverging spin-orbital coupling terms if the orbitals are determined variationally, but it is generally accepted that the applied approximation yields results within 5–10% of the experimental values if it is used in combination with scalar-relativistic wave functions.

All band-structure calculations were performed at the experimental equilibrium lattice constants a_0 at 300 K,[33] i.e., 5.869, 6.058, and 6.479 Å for InP, InAs, and InSb, respectively, although the effective masses, which we compare to in this study, have been measured at low temperature (roughly 4–30 K) by cyclotron resonance and Shubnikov-de Haas experiments. This approximation for the lattice constants seems to be reasonable since the linear thermal-expansion coefficients of In X are negligible (smaller than 5×10^{-6} K^{-1}). Unfortunately low-temperature lattice constants are not available for In X.

The parameters of the PAW potentials employed in this work, i.e., the core radii (R_{core}) and energy cutoffs (E_{cut}) as well as the states treated as valence states are summarized in Table I. In the present study, the semicore In $4d$ states were always treated as valence states and scalar-relativistic effects[32] were included during the pseudopotential generation. The theoretical lattice constants (a_0) and the bulk moduli (B_0) were determined by a fit to Murnaghan's equation of state,[34] where the energy was calculated at seven different volumes around the minimum in steps of $\Delta a = 0.1$ Å. In order to avoid effects from the changes in the size of the basis set, due to changes in the unit-cell volume, the energy cutoffs E_{cut} were increased by roughly 50% with respect to the energy cutoffs specified in Table I (400, 350, and 350 eV for InP, InAs, and InSb, respectively).

TABLE II. The theoretical lattice constants a_0 and bulk moduli B_0 calculated using different potentials (PAW and PAW+SOC) and xc functionals (PBE and the hybrid functional HSE06) compared to previously reported values obtained by the FP-LAPW method (Ref. 36) and experimental data from Refs. 33 and 39.

	InP		InAs		InSb	
Methods	a_0 (Å)	B_0 (GPa)	a_0 (Å)	B_0 (GPa)	a_0 (Å)	B_0 (GPa)
This work:						
PAW PBE	5.961	58.3	6.195	47.8	6.643	36.3
PAW+SOC PBE	5.959	58.4	6.194	47.9	6.645	36.0
PAW HSE06	5.904	68.4	6.114	56.8	6.561	43.0
PAW+SOC HSE06	5.902	69.0	6.114	56.6	6.564	42.5
Literature:						
FP-LAPW PBE (Ref. 36)	5.968	59.9	6.195	48.8		
Experiments (300 K):						
Ref. 33	5.8686	71.0	6.0584	58.0	6.4794	45.7
Ref. 39	5.8697		6.0583		6.4794	

The Brillouin-zone (BZ) integrations were carried out on Γ-centered k point meshes using the Gaussian smearing method with a width of 0.05 eV. For the equilibrium lattice constants and bulk moduli, $6\times6\times6$ k points were used, corresponding to a total of 16 irreducible k points in the first BZ.[35] In order to get accurate results for the band structures including SOC, no symmetry operations were employed, and the full mesh of k points corresponding to 216 k points was used.

The band structures $E(\mathbf{k})$ were computed on a discrete k mesh along high-symmetry directions, i.e., from the BZ center Γ with the coordinates (0,0,0) to the X point (1.0,0.0,0.0), L point (0.5,0.5,0.5), K point (0.75,0.75,0.00), and W point (1.0,0.5,0.0) in units of $(2\pi/a,2\pi/a,2\pi/a)$. The effective carrier masses m_e^*, m_{hh}^*, m_{lh}^*, and m_{so}^* were evaluated by fitting the conduction and the valence bands to a parabola according to $m^*=\frac{\hbar^2k^2}{2m_eE}$, where m_e denotes the electron rest mass. A k point spacing smaller than 0.02 $Å^{-1}$ was found to be required in order to suppress nonparabolic effects.

III. RESULTS AND DISCUSSION

A. Lattice constants and bulk moduli

The calculated lattice constants and the bulk moduli of In X are summarized in Table II. For comparison, previously reported results from other first-principles calculations and experimental data are included as well. We first emphasize the virtually perfect agreement between the PAW PBE results and the full-potential linearized-augmented plane-wave method (FP-LAPW) PBE results obtained using the WIEN-2K code.[36] This confirms that both methods are capable to obtain essentially exact results within the considered theoretical framework.

As usual for heavy elements, the PBE functional overestimates the lattice constants and the overestimation increases with increasing mass from 1.5% for InP, over 2.2% for InAs to 2.5% for InSb. As a result of the volume error, the bulk moduli are also significantly smaller than the experimental ones with errors increasing from 16% to 20%. The HSE06 functional clearly improves upon the PBE functional but still overestimates the lattice constants by 0.5%, 0.8%, and 1.2%, and for the bulk moduli the errors are 3% for InP and InAs and 7% for InSb. This is certainly a result and remainder of the PBE exchange-correlation functional, which yields large errors for the equilibrium volume for heavier elements. As usual SOC, changes the lattice constants very little (0.1%). In summary, the HSE06 functional improves the equilibrium volumes and the bulk moduli for In X, compared to the PBE functional, but a trend toward too large volumes prevails.

B. Electronic structures of In X

1. Band gaps

The fundamental band gaps and the split-off energies related to SOC are listed in Table III. In the absence of relativistic effects and spin splitting, the upper three valence bands are degenerated at the Γ point and made up by anion p states, whereas the electronlike conduction band is dominated by the In s orbital hybridized with the anion s orbital. The triple-degenerated valence band splits into a single-degenerated band and one double-degenerated band when moving away from Γ. As a matter of fact, there is no spin splitting and the bands are parabolic around Γ and symmetric in $\pm k$ due to time-reversal symmetry.[11,12]

In zinc blende, spin-orbit interactions modify the band topology around the Γ point significantly. When spin-orbit interactions are included, the six anion p states (three majority and three minority states) at the top of the valence band split into the split-off band at lower energies $(j=p-1/2,\Gamma_7^v)$ and four states at higher energy $(j=p+1/2,\Gamma_8^v)$.

TABLE III. Energy of the first conduction band $E_0(\Gamma_6^c-\Gamma_8^v)$, the second conduction band $E_0'(\Gamma_7^c-\Gamma_8^v)$, the valence band spin-orbit splitting (Δ_{SO}), and the second conduction band spin-orbit splitting (Δ_{SO}') evaluated at the Γ point. The PBE and the HSE06 results are compared to previously reported values, obtained using the FP-LAPW, GTO, LMTO, and experimental data from Refs. 33 and 39. Values computed without taking into account SOC, as well as including SOC are listed. All units are presented in eV.

	InP				InAs				InSb			
Methods	E_0	Δ_{SO}	E_0'	Δ_{SO}'	E_0	Δ_{SO}	E_0'	Δ_{SO}'	E_0	Δ_{SO}	E_0'	Δ_{SO}'
This work:												
PAW PBE	0.705		4.092		−0.188		3.898		−0.145		2.950	
PAW+SOC PBE	0.677	0.096	3.761	0.448	−0.298	0.341	3.479	0.455	−0.378	0.726	2.432	0.410
PAW HSE06	1.516		4.941		0.544		4.645		0.541		3.526	
PAW+SOC HSE06	1.481	0.114	4.607	0.441	0.420	0.382	4.217	0.449	0.284	0.791	2.986	0.411
PAW+G_0W_0+SOC(HSE06)	1.527		4.817		0.560		4.230		0.463		3.116	
PAW+$G_0W_0^{TC-TC}$+SOC(HSE06)	1.322		4.567		0.413		4.028		0.355		2.957	
Literature:												
FP-LAPW LDA (Ref. 7)	0.42				−0.51				−0.47			
GTO+SOC HSE03 (Ref. 40)	1.28	0.08			0.23	0.33			0.05	0.69		
LMTO+scQPGW+SOC (Ref. 13)	1.56	0.12	4.88	0.423	0.68	0.36	3.78	0.429	0.54	0.73	3.23	0.389
Experiments:												
Ref. 33 (at 300 K)	1.336	0.11	4.70	0.07	0.354	0.37			0.235	0.85	3.14	0.39
Ref. 39 (at 0 K)	1.424	0.108			0.417	0.39			0.235	0.81		

As usual, the spin-orbit splitting (Δ_{SO}) is defined as the energy difference between the split-off band and the four other states. In addition, zinc blende lacks inversion symmetry and after including SOC only parity-time-reversal symmetry prevails. Resultantly, the four remaining states at the top of the valence band split into two groups with different effective masses: the light-hole and the heavy-hole. This splitting is usually termed "Dresselhaus splitting" or the bulk inversion asymmetry splitting.[37]

On the PBE level our results clearly illustrate the problems one is faced with when using local or semilocal functionals. Whereas for InP, PBE predicts a one-electron band gap, the band order is inverted for InAs and InSb at the Γ point, i.e., the six anion p bands are located above the In s band. Inclusion of SOC worsens the description even further since heavy- and light-holes are pushed further up in energy. In the present calculations, the underestimation of the band gap is slightly less dramatic than for the FP-LAPW LDA calculations of Massidda *et al.*[7] The difference is mostly related to the use of a different DFT functional in the present work. Using the LDA, our band gaps are predicted to be 0.48, −0.42, and −0.37 eV for InP, InAs and InSb, now consistently 0.1 eV greater than the values obtained by Massidda *et al.* The remaining discrepancy might be related to insufficient basis set convergence of the FP-LAPW calculations (performed in 1990). The error of the available density functionals is usually attributed to too shallow In d electrons pushing up the anion p bands (p-d repulsion). The problem can be reduced somewhat by placing the d electrons in the core but even then "negative" band gaps are predicted for InAs and InSb using the PAW method.

HSE06 repairs the deficiency entirely and restores the correct band order at the Γ point. To obtain good agreement with experiment, SOC has to be included now, in particular for the heavier anions, since the hybridization between In $5p$ and anion p states increases significantly from InP to InSb,[7,38] and because spin-orbit splitting within the anion p shell also increases with increasing anion mass. The SO splitting, Δ_{SO}, is calculated to be 0.114, 0.382, and 0.791 eV for InP, InAs, and InSb, respectively. These values are in excellent agreement with the results of angle-resolved photoemission experiments, i.e., 0.108 eV (InP), 0.39 eV (InAs), and 0.81 eV (InSb).[39] The agreement with the fully relativistic LMTO values of Cardona *et al.* (0.108 and 0.803 eV for InP and InSb, respectively)[12] is also excellent, whereas Chantis *et al.* (row LMTO+scQPGW+SOC) (Ref. 13) underestimated the SO splitting somewhat, most likely because they treated the spin-orbit operator only as a perturbation, but did not include it in the self-consistency cycle.

After inclusion of SOC, the band gaps of InP and InAs are practically identical with experiment, whereas that of InSb is slightly overestimated (0.284 eV compared to 0.24 eV; 20% error). In Ref. 40, which adopted the Gaussian-type orbitals (GTO) method, (row GTO+SOC), the HSE03 functional was applied, which uses a larger screening parameter of $\mu=0.3$ Å^{-1} resulting in a much smaller gap. For most materials, the HSE06 functional ($\mu=0.2$ Å^{-1}) performs better than the older functional. The strong dependence on the screening parameter μ, however, demonstrates that the good agreement achieved in the present work is certainly to some extent fortuitous; nevertheless, HSE06 predicts good band gaps rather systematically across the periodic table[22–24,31] including even ternary and quaternary compounds.[28] The position of the second conduction band E_0' is also well predicted using HSE06, although a slight tendency toward too small values is visible.

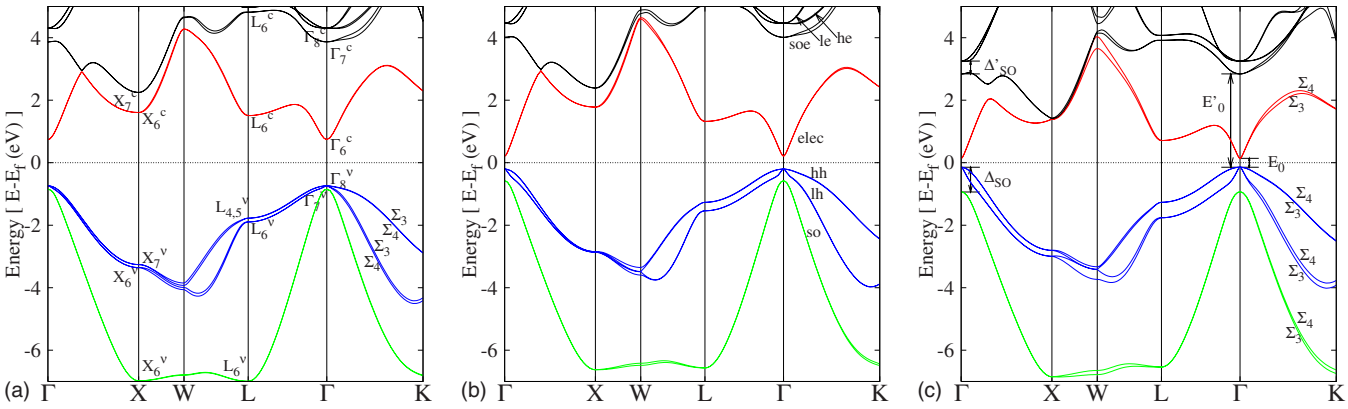

FIG. 1. (Color online) The band structures of (a) InP, (b) InAs, and (c) InSb along Γ-*X*-*W*-*L*-Γ-*K* obtained from PAW HSE06 calculations (including SOC). The electronlike conduction band (elec), heavy-hole (hh), light-hole (lh), and split-off (so) bands are shown. The Fermi level is indicated by the horizontal doted line.

The spin-orbit splitting for the second conduction band also compares well with the experimental data for InSb. The experimental value for InP is most likely inaccurate and not supported by ours or the LMTO+scQP*GW* calculations.

On top of the HSE06 calculations, the single-shot G_0W_0 calculations were performed, and the results are also included in Table III. SOC was not included in these calculations and only added *a posteriori* using the values obtained for the HSE06 functional. Using a simple single-shot G_0W_0 calculation, starting from HSE06 wave functions and eigenvalues, too large band gaps were found, a trend that has also been observed for other materials.[41,42] This is related to the fact that the HSE06 functional predicts too small dielectric constants if the random-phase approximation is used (as it is commonly done in the *GW* approximation).[42] Similar observations are made in the self-consistent quasiparticle *GW* (LMTO+scQP*GW*) method of Chantis *et al.*, which also tends to overestimate the band gaps.[13] Considering that a technical accuracy of 0.1 eV is difficult to attain using *GW* methods, our results compare well with these scQP*GW* calculations. The overestimation can be almost entirely removed by including the electrostatic interaction between electron and holes in the calculation of the screening properties ϵ, which enter $W=\epsilon^{-1}v$, where v is the bare Coulomb kernel. The corresponding results are reported in the row $G_0W_0^{\text{TC-TC}}$. Except for InSb, the results are now in good agreement with experiment. For InSb, we believe that the error is related to the neglect of SOC in the calculation of the dielectric properties: SOC lowers the split-off band and raises the heavy-hole and light-hole bands, on average conserving the center of mass. As long as the SO splitting is small compared to the band gap, it is reasonable to approximate the eigenvalues by the center of mass (i.e., neglecting SOC). But when the SO splitting approaches the value of the band gap, the influence of SOC on the screening properties can no longer be neglected and should be taken into account. A similar observation was also made for PbTe *GW* calculations.[24] Unfortunately our *GW* code currently does not allow for a consistent inclusion of SOC.

In summary, it is obvious that the *GW* approach hardly yields quantitatively more accurate results than the HSE06 functional. Even though the HSE06 functional lacks the fundamental justification of the *GW* method, it is fairly clear that HSE06 allows for a very accurate description of the band gaps, without going through all the complications of sophisticated many-electron calculations (which in the present case would even require vertex corrections in *W*). Using the HSE06 functional, the calculation of the effective masses is also much more straightforward, and we will, therefore, limit the following calculations to the HSE06 functional.

2. Band structure

The band structures of the In *X* semiconductors were calculated using the HSE06 functional including SOC. In Fig. 1, the In *X* band structures are shown in an energy range from −7 to 5 eV and drawn along the important high-symmetry lines. The results are fairly similar to those of Cardona *et al.*[12] who used an LMTO approach with muffin-tin potentials that were empirically adjusted to fit the experimental band gaps. Since SOC was included in the calculations, the SO splitting is clearly visible in the valence and the conduction bands. The maximum SO splitting for the valence band and the conduction band was found at *L* and *X*, respectively. One qualitative difference is that the first and the second conduction bands along Γ*X* seem to cross in InP and InAs, whereas Cardona *et al.* observed a clear level repulsion resulting in a forbidden crossing.[12] Using a purely local functional (PBE) we find good agreement with Cardona with a forbidden crossing. In principle, the "crossing" is a result of an interchange of the order at *X* compared to the Γ point, i.e., at the *X* point the In p_x orbital (X_6^c) is below the In *s* orbital (X_7^c), whereas at Γ the In *s* orbital makes up the conduction band edge (Γ_6^c state). Nevertheless, since the two bands belong to the same irreducible representation along $\Gamma X(\Delta_5)$,[37] the matrix element between the two states is not necessarily zero and the crossing is in principle forbidden. The matrix element in the HSE case is negligible resulting—within the limits of our calculational accuracy—into a crossing. A similar observation is made for InAs.

Due to the absence of inversion symmetry in the zinc-blende In *X* semiconductors, the degeneracy between spin up and spin down is lifted for the electron band, the heavy-hole,

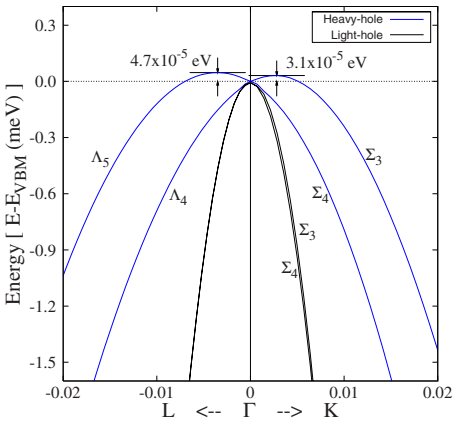

FIG. 2. (Color online) Close-up of the band structure of InP near the Γ point along Γ*L*[111] and Γ*K*[110]. The linear dispersion of heavy-hole with a maximum on off Γ is clearly visible. The results are from PAW+SOC HSE06 calculations.

the light-hole, and the split-off band at lower symmetry points even in the absence of a macroscopic magnetic field.[12,37] Furthermore, the heavy-hole states show a linear dispersion with a maximum slightly off Γ. The band structure in the vicinity of the Γ point is illustrated for InP in Fig. 2 for the HSE06 functional. Experimentally, the hole subband splitting of InSb has been intensively investigated by Robinson[43] and Pidgeon and Groves[44,45] through the measurements of the cyclotron resonance of holes. Theoretical calculations for the subband splitting of the hole and the electron bands have been presented by Cardona *et al.*,[12] whereas theoretical studies of the splitting within the electron band have been reported by many researchers.[11,13,46,47]

The largest subband splitting was observed at the *W* point for all In *X* (see Fig. 1). Details for the subband splitting within the electron band and within the three holelike bands are shown in Fig. 3 along the high-symmetry lines from Γ to *L* ([111] direction) and from Γ to *K* ([110] direction). The values were obtained by calculating the energy difference between the Σ_4 and the Σ_3 states, where the splitting will be designated as positive if the Σ_4 state is above Σ_3. The subband splitting shows a remarkable complex topology, which is driven by a subtle interplay between hybridization between conduction and valence bands and SOC. Along Γ*K* the Σ_3 and the Σ_4 bands sometimes even cross (i.e., whenever the difference crosses zero in Fig. 3). Our results are remarkably similar to those of the fully relativistic calculations of Cardona *et al.*, both for the absolute magnitude of the spin splitting, as well as for the positions at which spin-up and spin-down states cross.[12] For InSb, for instance, the maximal intraband splitting is 165 meV exactly identical to the value of Cardona *et al.*, the subband splitting for the electron reaches 135 meV and that for the split-off band is 125 meV, all values match closely those of Cardona *et al.* For the heavy-hole splitting in InSb, we observe, also in agreement with Cardona *et al.*, a crossing briefly after the Γ point along Γ*K*.

Using the *GW* method, Chantis *et al.* generally observed somewhat smaller SO splittings.[13] This is most likely related to their non-self-consistent perturbational SOC treatment, which always slightly underestimates the SO splitting (see also Table III). For instance, for the electron in InSb, their maximal subband splitting is only 120 meV, compared to 135 meV in the present work and in the work of Cardona *et al.* Finally, it is noted that our present results also agree well with the experimental results of Robinson.[43] In summary, the PAW method recovers the fully relativistic results exceedingly well, suggesting that if full self-consistency is achieved, very accurate results can be obtained in spite of the second-order SOC treatment used here.

3. Effective charge-carrier masses

In Table IV, the results for the effective electron and hole masses are summarized for the HSE06 functional for the directions Γ*X*[100], Γ*K*[110], and Γ*L*[111]. For comparison, the experimental values from Ref. 39 are listed, and furthermore, as an example, the PBE results for InP are included as well. As already emphasized the masses were evaluated numerically by fitting the calculated dispersion curves around the Γ point. Independent fits for all three directions were performed, although only a small set of effective masses are linearly independent. For instance, for symmetry reasons the split-off mass and the electron mass are identical along all three directions. Within $0.001m_e$ this is indeed observed in our calculations. However, even more linear dependencies

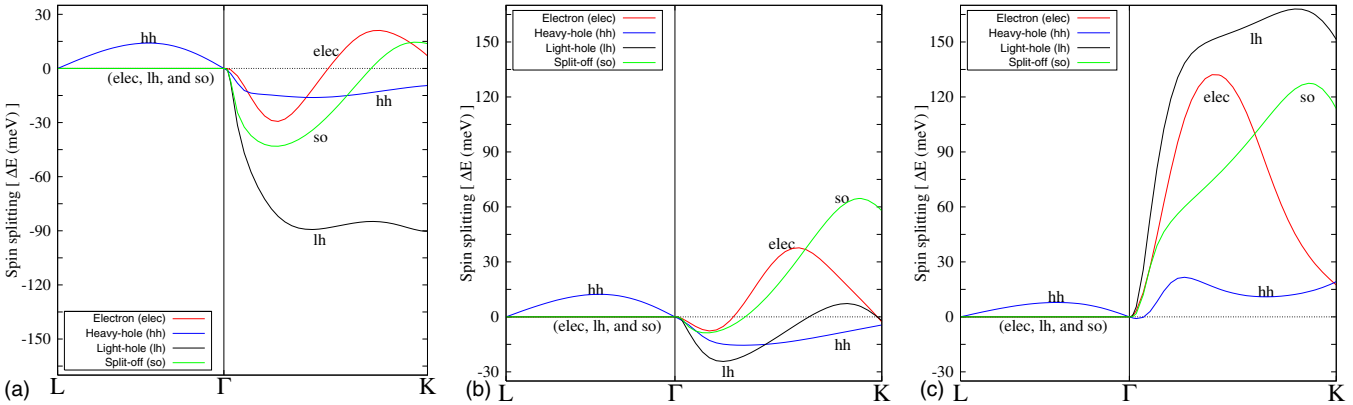

FIG. 3. (Color online) Subband spin splitting of electron conduction band (elec), heavy-hole (hh), light-hole (lh), and split-off band (so) along Γ*L*[111] and Γ*K*[110] for (a) InP, (b) InAs, and (c) InSb. The results are from PAW+SOC HSE06 calculations.

TABLE IV. Effective hole and electron masses at the Γ point in units of the electron rest mass m_e calculated using the HSE06 functional with spin-orbit coupling. For comparison, the PAW PBE results are given for InP. The experimental values were calculated from the Luttinger parameter tabulated in Ref. 39.

Elements	Directions	$\lvert m^*_{\text{split-off}}/m_e\rvert$	$\lvert m^*_{\text{light-hole}}/m_e\rvert$	$\lvert m^*_{\text{heavy-hole}}/m_e\rvert$	$\lvert m^*_{\text{electron}}/m_e\rvert$
PAW+SOC_PBE:					
InP	[100]	0.142	0.075	0.438	0.055
	[111]	0.142	0.068	1.016	0.055
	[110]	0.142	0.070	0.779	0.056
PAW+SOC_HSE06:					
InP	[100]	0.192	0.117	0.414	0.089
	[111]	0.193	0.101	0.944	0.089
	[110]	0.193	0.104	0.738	0.089
InAs	[100]	0.112	0.033	0.343	0.027
	[111]	0.111	0.031	0.836	0.027
	[110]	0.112	0.032	0.623	0.027
InSb	[100]	0.132	0.021	0.244	0.019
	[111]	0.132	0.020	0.627	0.019
	[110]	0.132	0.020	0.455	0.019
Experiment:					
InP	[100]	0.210	0.121	0.531	0.080
	[111]	0.210	0.108	1.136	0.080
	[110]	0.210	0.111	0.885	0.080
InAs	[100]	0.140	0.027	0.333	0.026
	[111]	0.140	0.037	0.625	0.026
	[110]	0.140	0.026	0.513	0.026
InSb	[100]	0.110	0.015	0.263	0.014
	[111]	0.110	0.015	0.556	0.014
	[110]	0.110	0.015	0.435	0.014

exist, and it is possible to determine all effective hole masses from the three Luttinger parameters:[39,48]

$$\left(\frac{m^*_{hh}}{m_e}\right)^{[100]} = \frac{1}{\gamma_1 - 2\gamma_2},$$

$$\left(\frac{m^*_{hh}}{m_e}\right)^{[110]} = \frac{2}{2\gamma_1 - \gamma_2 - 3\gamma_3},$$

$$\left(\frac{m^*_{hh}}{m_e}\right)^{[111]} = \frac{1}{\gamma_1 - 2\gamma_3},$$

$$\left(\frac{m^*_{lh}}{m_e}\right)^{[100]} = \frac{1}{\gamma_1 + 2\gamma_2},$$

$$\left(\frac{m^*_{lh}}{m_e}\right)^{[110]} = \frac{2}{2\gamma_1 + \gamma_2 + 3\gamma_3},$$

$$\left(\frac{m^*_{lh}}{m_e}\right)^{[111]} = \frac{1}{\gamma_1 + 2\gamma_3}. \quad (5)$$

The Luttinger parameters were obtained by a least-square fit of the effective carrier masses and are presented in Table V. The mean absolute errors in the least-square fit were 0.02, 0.04, and 0.15 for InP, InAs, and InSb, respectively, and recalculating the effective masses from the Luttinger parameters gave results within 0.001 of those reported in Table IV. This shows that the present results are numerically accurate, although systematic errors introduced by the functional are another matter.

Comparison with experiment is most straightforward using the Luttinger parameters. For InP, agreement with experiment is excellent and most likely close to the accuracy of the experiments, but it is also clear that errors increase with increasing anion mass. For InAs, the Luttinger parameters are about 18% too small and the error increases to almost 26% for InSb. As shown above [Eq. (5)] the Luttinger parameters are essentially inverse proportional to the effective masses and clearly those effective masses that are small are significantly overestimated for InSb (and less so for InAs). But the

TABLE V. Luttinger parameters of In X semiconductors. The values were determined by a least-square fit to the effective masses in Table IV. The experimental Luttinger parameters are from Ref. 39.

Elements	γ_1	γ_2	γ_3
This work:			
InP	5.48	1.54	2.22
InAs	16.5	6.77	7.64
InSb	26.0	10.9	12.2
InSb (μ=0.23)	29.7	12.7	14.1
Experiment:			
InP	5.08	1.60	2.10
InAs	20.0	8.5	9.2
InSb	34.8	15.5	16.5

trends are not as systematic in the effective masses.

The small effective masses are a result of the strong level repulsion between the valence band holes and conduction band electrons: at the Γ point, a direct interaction between the *s*-like conduction band and the *p*-like valence band is forbidden, but slightly off Γ the interaction is allowed by symmetry. The interaction energy is inverse proportional to the square of the band gap, resulting in a very strong level repulsion between the light-hole and the electron band for small gap semiconductors. A good prediction of the electronic masses is easy for large gap materials but becomes increasingly difficult when the band gap closes since even tiny errors in the band gap will cause a large error in the predicted effective masses. InSb is the most critical case since HSE06 predicts a band gap that is 20% larger than the experimental one. To access how a change in the band gap will affect the effective masses, the screening parameter was changed from μ=0.2 to μ=0.23 in the HSE functional and the band gap and the effective masses were re-evaluated. Using this setting, the band gap is reduced to the experimental value of 0.239 eV and the Luttinger parameters increase as shown in Table V. The error is now about 15%, similar to that for InAs. This clearly indicates that part of the error in InSb is related to the too large HSE06 band gap but the larger part of the error still prevails, as for InAs, where the HSE06 functional predicts the band gap accurately.

It is difficult to determine the reason for the remaining discrepancy but we remark that Cardona *et al.* also found too large effective masses ($k\|[110]$) for the light-hole ($0.019m_e$) and the electron ($0.016m_e$) for InSb.[12] These values agree almost perfectly with our values for μ=0.23: $0.017m_e$ (light-hole) and $0.0165m_e$ (electron). This suggests that (i) hybrid functionals and local functionals predict very similar matrix elements and (ii) hence if the band gaps are identical, identical effective masses are obtained. This observation, *a posteriori*, justifies the use of semiempirical muffin-tin potentials fitted to reproduce the experimental band gap. The discrepancy between experiment and theory for the effective masses, however, remains unexplained, since the semiempirical LMTO calculations and the HSE06 calculations give identical effective masses when the parameters are adjusted to fit the experimental band gaps. A possible reason for the remaining discrepancy might be errors in the experimental values or electron-phonon coupling neglected in our and most theoretical treatments.

IV. CONCLUSIONS

In this paper, the structural and the electronic properties of narrow-gap In X semiconductors were calculated using the screened hybrid functional HSE06 and spin-orbit coupling. Using a conventional gradient corrected density functional, PBE, the lattice constants are overestimated compared to experiment, resulting in significantly underestimated bulk moduli. The hybrid functional, HSE06, gives a more balanced description of the lattice parameters and bulk moduli with a slight overestimation of the lattice constants (1% on average) and a slight underestimation of the bulk moduli, 3% in the case of InP and InAs, and 7% for InSb.

For the electronic properties, PBE fails entirely for InAs and InSb with an incorrect band order at the Γ point and much too small band gaps for InP. Resultantly, the effective masses are only in modest agreement with experiment for InP. This indicates that a naive scissor correction, causing a rigid up shift of the conduction band, is not sufficient to describe subtleties of the band topology. For the band gaps, the HSE06 functional yields exceptionally good results if spin-orbit coupling is included. The largest errors are observed for InSb, where the band gap is overestimated by about 20% (or 40 meV). The predicted effective masses are in very good agreement with experiment for InP but are generally overestimated for InAs and InSb. Concomitantly, the Luttinger parameters, which are inversely proportional to the effective masses, are accurate for InP but underestimated by 18% and 26% for InAs and InSb. In InSb, part of the error is clearly related to the overestimation of the band gap. We have illustrated this by slightly increasing the screening length (μ) in the HSE06 functional, which in turn decreases the band gap and the Luttinger parameters. However, a 15% error in the Luttinger parameters and the effective masses prevails in InSb and InAs, even if the functional predicts the correct band gap. For more accurate predictions quasiparticle methods might be required, but it is also possible that other effects, such as coupling to zero-point vibrations, might influence the effective masses. Altogether, the present study demonstrates that hybrid functionals are a very valuable and efficient tool to study intricate details of the band topology and effective masses. They clearly outperform traditional semilocal density functionals and predict effective masses within 15% of experiment if the band gap is tuned to fit the experimentally measured values. We believe that this method can be valuable for the prediction of effective masses in materials where experimental dates are not available.

We finally note that the present study *a posteriori* justifies the use of empirically adjusted one-electron Kohn-Sham potentials for the prediction of effective masses and other band-topology-related parameters. Cardona *et al.* added a sharply peaked potential at the atomic sites in order to reproduce the experimental band gaps.[12] Their spin-orbit splittings, effec-

tive masses, and Luttinger parameters are within few percent of our values derived by an essentially parameter free approach. Empirical corrections to the Kohn-Sham potentials are obviously able to predict accurate band topologies without resorting to computationally demanding hybrid functionals or elaborated many electron techniques such as *GW*.

ACKNOWLEDGMENTS

This work was supported by the Austrian Fonds zur Förderung der Wissenschaftlichen Forschung within the special research program "Infrared Optical Nanostructures (IR-ON)" and within the START Project No. Y218.

*yoon-suk.kim@univie.ac.at; http://cms.mpi.univie.ac.at/

[1] M. Razeghi, Nature (London) **369**, 631 (1994).
[2] S.-W. Kim, S. Sujith, and B. Y. Lee, Chem. Commun. (Cambridge) **2006**, 4811
[3] A. R. J. Marshall, C. H. Tan, M. J. Steer, and J. P. R. David, Appl. Phys. Lett. **93**, 111107 (2008).
[4] J. R. Chelikowsky and M. L. Cohen, Phys. Rev. B **14**, 556 (1976).
[5] K. J. Chang, S. Froyen, and M. L. Cohen, Solid State Commun. **50**, 105 (1984).
[6] I. Gorczyca, N. E. Christensen, and M. Alouani, Phys. Rev. B **39**, 7705 (1989).
[7] S. Massidda, A. Continenza, A. J. Freeman, T. M. de Pascale, F. Meloni, and M. Serra, Phys. Rev. B **41**, 12079 (1990).
[8] X. Zhu and S. G. Louie, Phys. Rev. B **43**, 14142 (1991).
[9] J. Heyd, G. E. Scuseria, and M. Ernzerhof, J. Chem. Phys. **118**, 8207 (2003).
[10] L. Hedin, Phys. Rev. **139**, A796 (1965).
[11] W. Zawadzki and P. Pfeffer, Semicond. Sci. Technol. **19**, R1 (2004).
[12] M. Cardona, N. E. Christensen, and G. Fasol, Phys. Rev. B **38**, 1806 (1988).
[13] A. N. Chantis, M. van Schilfgaarde, and T. Kotani, Phys. Rev. Lett. **96**, 086405 (2006).
[14] G. Kresse and J. Furthmüller, Comput. Mater. Sci. **6**, 15 (1996).
[15] P. E. Blöchl, Phys. Rev. B **50**, 17953 (1994).
[16] G. Kresse and D. Joubert, Phys. Rev. B **59**, 1758 (1999).
[17] J. P. Perdew, K. Burke, and M. Ernzerhof, Phys. Rev. Lett. **77**, 3865 (1996).
[18] J. Paier, R. Hirschl, M. Marsman, and G. Kresse, J. Chem. Phys. **122**, 234102 (2005).
[19] M. Shishkin and G. Kresse, Phys. Rev. B **74**, 035101 (2006).
[20] M. Shishkin, M. Marsman, and G. Kresse, Phys. Rev. Lett. **99**, 246403 (2007).
[21] J. Heyd and G. E. Scuseria, J. Chem. Phys. **121**, 1187 (2004).
[22] J. Paier, M. Marsman, K. Hummer, G. Kresse, I. C. Gerber, and J. G. Ángán, J. Chem. Phys. **124**, 154709 (2006).
[23] J. Paier, M. Marsman, K. Hummer, G. Kresse, I. C. Gerber, and J. G. Ángán, J. Chem. Phys. **125**, 249901 (2006).
[24] K. Hummer, A. Grüneis, and G. Kresse, Phys. Rev. B **75**, 195211 (2007).
[25] R. O. Jones and O. Gunnarsson, Rev. Mod. Phys. **61**, 689 (1989).
[26] P. Mori-Sanchez, A. J. Cohen, and W. T. Yang, Phys. Rev. Lett. **100**, 146401 (2008).
[27] J. Muscat, A. Wander, and N. M. Harrison, Chem. Phys. Lett. **342**, 397 (2001).
[28] J. Paier, R. Asahi, A. Nagoya, and G. Kresse, Phys. Rev. B **79**, 115126 (2009).
[29] B. G. Janesko, T. M. Henderson, and G. E. Scuseria, Phys. Chem. Chem. Phys. **11**, 443 (2009).
[30] K. Hummer and G. Kresse (unpublished).
[31] A. V. Krukau, O. A. Vydrov, A. F. Izmaylov, and G. E. Scuseria, J. Chem. Phys. **125**, 224106 (2006).
[32] R. J. Elliott, Phys. Rev. **96**, 266 (1954).
[33] *Landolt-Börnstein Semiconductors*, edited by O. Madelung, U. Rössler, and M. Schulz (Springer-Verlag, Berlin, 2002), Vol. 41A1b.
[34] F. F. Murnaghan, Proc. Natl. Acad. Sci. U.S.A. **30**, 244 (1944).
[35] H. J. Monkhorst and J. D. Pack, Phys. Rev. B **13**, 5188 (1976).
[36] F. Tran, R. Laskowski, P. Blaha, and K. Schwarz, Phys. Rev. B **75**, 115131 (2007).
[37] G. Dresselhaus, Phys. Rev. **100**, 580 (1955).
[38] P. Carrier and S.-H. Wei, Phys. Rev. B **70**, 035212 (2004).
[39] I. Vurgaftman, J. R. Meyer, and L. R. Ram-Mohan, J. Appl. Phys. **89**, 5815 (2001).
[40] J. E. Peralta, J. Heyd, G. E. Scuseria, and R. L. Martin, Phys. Rev. B **74**, 073101 (2006).
[41] F. Fuchs, J. Furthmüller, F. Bechstedt, M. Shishkin, and G. Kresse, Phys. Rev. B **76**, 115109 (2007).
[42] J. Paier, M. Marsman, and G. Kresse, Phys. Rev. B **78**, 121201(R) (2008).
[43] M. L. A. Robinson, Phys. Rev. Lett. **17**, 963 (1966).
[44] C. R. Pidgeon and S. H. Groves, Phys. Rev. Lett. **20**, 1003 (1968).
[45] C. R. Pidgeon and S. H. Groves, Phys. Rev. **186**, 824 (1969).
[46] S. Shokhovets, O. Ambacher, and G. Gobsch, Phys. Rev. B **76**, 125203 (2007).
[47] J.-W. Luo, G. Bester, and A. Zunger, Phys. Rev. Lett. **102**, 056405 (2009).
[48] J. M. Luttinger and W. Kohn, Phys. Rev. **97**, 869 (1955).